Available online at www.sciencedirect.com
ScienceDirect
Journal of the European Ceramic Society 30 (2010) 1765–1774
www.elsevier.com/locate/jeurceramsoc

Microstructural characterization of ceramic–intermetallic composites using TEM related techniques

M.J. Sayagués *, M.A. Avilés, J.M. Córdoba, M.D. Alcalá, F.J. Gotor

Instituto de Ciencia de Materiales de Sevilla, Centro mixto CSIC-US, Av. Américo Vespucio 49, 41092 Sevilla, Spain

Received 5 October 2009; received in revised form 12 January 2010; accepted 27 January 2010
Available online 2 March 2010

Abstract

TiC_xN_y/Ti–Ni and TiC_xN_y/Ti–Co composites formed by ceramic and intermetallic binder phases were produced by pressureless sintering at 1400 °C from powders synthesized by a mechanically induced self-sustaining reaction (MSR) process. Four different composites were characterized using high-resolution electron microscopic techniques, in both scanning (SEM, HRSEM) and transmission (TEM, HRTEM, ED, EDS and EELS) modes and using an energy filtered technique (EFTEM) associated with electron energy loss spectroscopy (EELS). The microcharacterization showed that the ceramic phase with an *fcc*-cubic structure displayed a short-range order in many crystals detected by diffuse scattering in the ED patterns. This was possibly due to a sequence of C, N, and vacancies of both atoms along certain directions in the structure. On the other hand, even though the binder phase was introduced as metal in the reaction process, it was formed by Ni–Ti or Co–Ti known intermetallic compounds ($NiTi_2$, Ni_3Ti, and Co_3Ti). An unknown Ni–Ti intermetallic structure with a Ni:Ti ratio close to 2:1 was only found in one of the synthesized composites and displayed a cubic structure with a lattice parameter, *a*, of about 8.7 Å.

Keywords: A. Milling; B. Microstructure-final; D. Carbides and nitrides; E. Structural applications

1. Introduction

TiC_xN_y-based cermets (ceramic–metal composites) are materials of great interest in both fundamental investigation and practical applications, and they have been considered as substitutes for the conventional WC-based hard metals in the metal cutting industry due to their excellent combination of mechanical properties.[1,2] Hardness, toughness, wear resistance of TiC_xN_y-based cermets, and their resulting performance are influenced by both ceramic and metal (or binder) phases and can be improved by optimizing the microstructure and the material composition.[3] On the other hand, the chemical and physical properties (e.g., microhardness, electrical and heat conductivity, shear modulus[4,5]) of the TiC_xN_y ceramic phase, which is a solid solution between titanium carbide (TiC) and titanium nitride (TiN), rely on their C and N stoichiometry. Additionally, it has been shown that, in these composites, the shape and size of the ceramic particles after the liquid phase sintering are dependent on the C/N ratio.[6,7]

Several studies[8,9] have revealed that the best way to improve the properties of TiC_xN_y-based cermets is to reduce the grain size of the hard phase and to increase the homogeneity of the structural elements. Both features depend dramatically on the method of preparation. We have shown that the mechanochemical process known as mechanically induced self-sustaining reaction (MSR) allows the synthesis of TiC_xN_y-based powdered composites with nanometric character and excellent dispersion of the tough binder around the hard particles.[10] This method also permits the production of nanocrystalline carbonitride powders with homogeneous and controlled chemical composition (tailored C/N ratio) by adequately adjusting the milling parameters and the metal-to-carbon atomic ratio in the starting mixture.[11,12]

We have previously suggested that the optimal combination of properties found in TiC_xN_y-based cermets obtained by MSR and sintered by a pressureless method was due to the homogeneous chemical composition and microstructure developed during processing.[13] The present work focused on the detailed analysis of these two features (key factors to

* Corresponding author.
E-mail address: sayagues@cica.es (M.J. Sayagués).

0955-2219/$ – see front matter © 2010 Elsevier Ltd. All rights reserved.
doi:10.1016/j.jeurceramsoc.2010.01.039

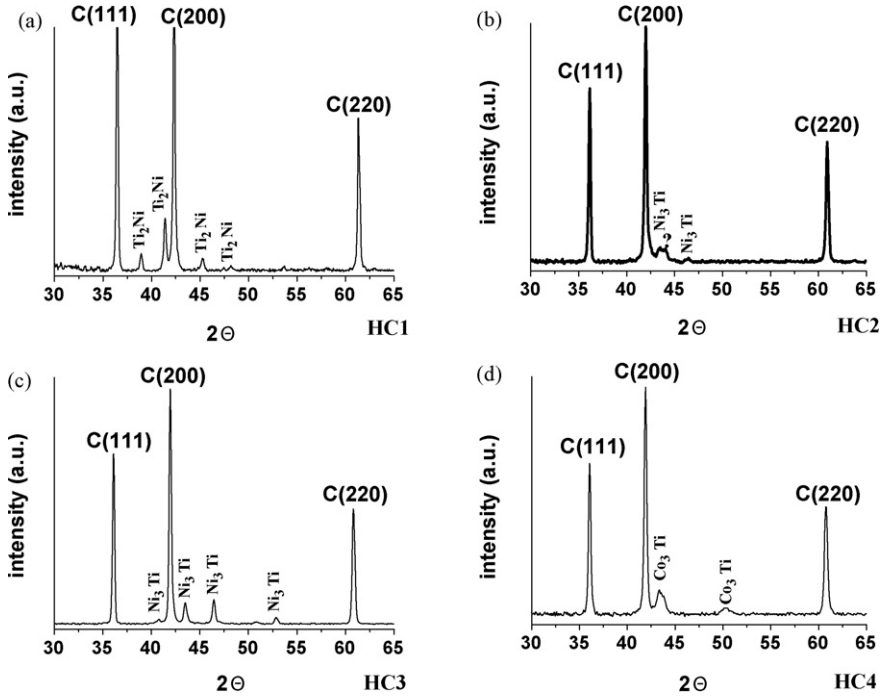

Fig. 1. X-ray diffraction patterns corresponding to the four composites: (a) HC1; (b) HC2; (c) HC3 and (d) HC4. The ceramic phase peaks (C) with the corresponding (*h k l*) index are marked and the intermetallic phases are identified. The peak marked with a "?" in the HC2 sample could not be assigned.

obtain improved properties) at a microscopic level by means of electron microscopy-related techniques: scanning electron microscopy and high-resolution scanning electron microscopy (SEM and HRSEM), transmission electron microscopy and high-resolution transmission electron microscopy (TEM and HRTEM), electron diffraction (ED), energy dispersive X-ray spectroscopy (EDS), electron energy loss spectroscopy (EELS), and energy filtered transmission electron microscopy (EFTEM).

2. Experimental

Titanium powder (99% in purity, <325 mesh, Strem Chemicals), graphite powder (<270 mesh, Fe ≤ 0.4%, Merck), nickel powder (puriss., Fluka), and cobalt powder (99.9% in purity, <100 mesh, Sigma) were used in this work. Powdered composites were obtained in one step by MSR from elemental powder mixtures under a nitrogen atmosphere (H_2O and $O_2 \leq 3$ ppm) using a modified planetary ball mill (model Micro Mill Puverisette 7, Fritsch, Idaroberstein, Germany).

The metal binder, Ni or Co, was added to the titanium/graphite mixture that is necessary to form the TiC_xN_y hard phase before the MSR process was performed. More details of the preparation method can be found elsewhere.[10] Four different composites were synthesized using the following Ti:C atomic ratios and weight percentages of metal: Ti:C = 1:0.25, 15 wt% Ni (HC1); Ti:C = 1:0.50, 15 wt% Ni (HC2); Ti:C = 1:0.75, 15 wt% Ni (HC3); and Ti:C = 1:0.50, 15 wt% Co (HC4).

Powdered composites were isostatically cold-pressed at 200 MPa during 5 min to give cylinders of 12 mm in diameter and 45 mm in height. The green bodies were sintered without pressure at 1400 °C for 60 min (heating rate 10 °C/min, free cooling) under inert atmosphere (helium gas, $H_2O \leq 3$ ppm, $O_2 \leq 2$ ppm and $C_nH_m \leq 0.5$ ppm, Air Liquid) in a horizontal furnace (Thermolyne Type 59300 model no. F-59340-CM, Thermolyne).

X-ray diffraction patterns of the polished surfaces of the consolidated composites were obtained with a Philips X'Pert Pro instrument equipped with a Θ/Θ goniometer using Cu Kα radiation (40 kV, 40 mA), a secondary K_β filter, and an X'Celerator detector. The diffraction patterns were scanned from 30° to 130° (2Θ) at a scanning rate of 0.42° min^{-1}. Silicon powder (NIST) was used to correct XRD shift peaks.

Thin disks (3 mm Ø) of the consolidated composites were subsequently prepared by cutting, polishing, dimpling, and ion milling (DuoMill, Gatan Inc.). Microcharacterization was performed using the following techniques and equipments:

- Scanning electron microscopy (SEM) with a ***PHILIPS XL-30*** (resolution 3.5 nm) and high-resolution scanning electron microscopy (HRSEM) with a ***HITACHI S5200*** with a field emission gun (FEG) (resolutions of 0.4 nm at 30 kV and 1.6 nm at 1 kV) (Seville University, CITIUS Centre).

Table 1
Lattice parameter, ***a***, and the estimated stoichiometry for the TiC_xN_y ceramic phase, and binder phases present in each consolidated composite observed by XRD.

Composites	*a* (Å)	TiC_xN_y composition by XRD (Vegard's law)	Binder phase
HC1	4.2705	$TiC_{0.36}N_{0.64}$	Ti_2Ni
HC2	4.3037	$TiC_{0.75}N_{0.25}$	Ni_3Ti
HC3	4.3071	$TiC_{0.79}N_{0.21}$	Ni_3Ti
HC4	4.3125	$TiC_{0.85}N_{0.15}$	Co_3Ti

- Transmission electron microscopy (TEM), electron diffraction (ED), energy dispersive X-ray spectroscopy (EDX), and electron energy loss spectroscopy (EELS) with a ***PHILIPS CM200***, LaB_6 filament (Seville, ICMS). EELS spectra were acquired with a Gatan model 766-2K parallel detection electron spectrometer and were recorded in the diffraction mode with a collection angle of 1.45 mrad. The measured energy resolution at the zero-loss peak of the coupled microscope/spectrometer system was about 2 eV. A low-loss spectrum was also recorded with each edge in the same illuminated area. After background subtraction with a standard power law function, the spectra were deconvoluted for plural

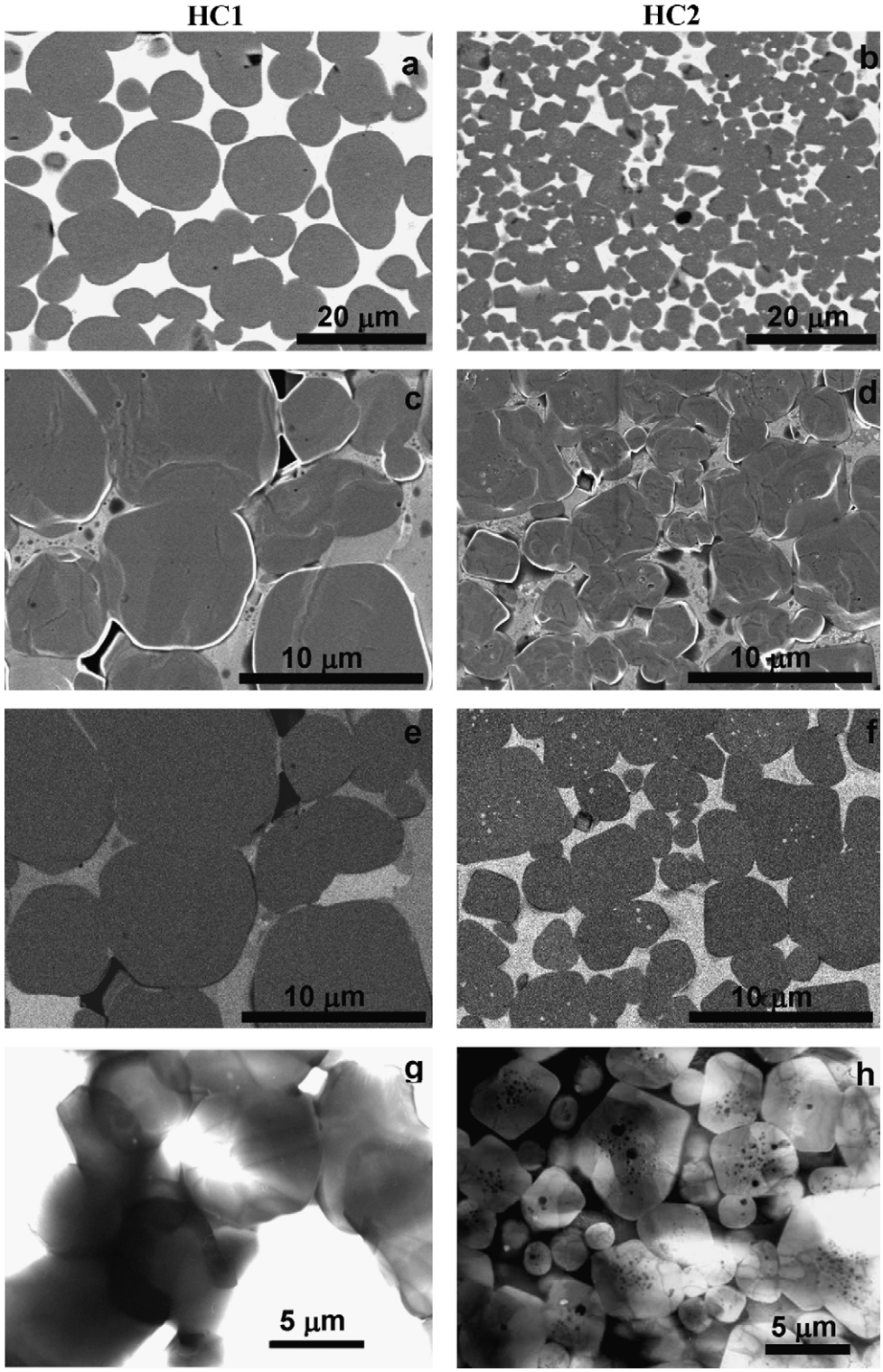

Fig. 2. Micrographs corresponding to HC1 and HC2 composites. (a and b) SEM images taken with secondary electrons. (c and d) HRSEM images taken with secondary electrons and (e and f) with backscattered electrons. (g and h) Bright field TEM images.

scattering with the Fourier-ratio method. All these treatments were performed within the EL/P program (Gatan).

- High-resolution transmission electron microscopy (HRTEM) with a ***JEOL JEM 3010***, LaB_6 filament (Cs = 0.6 mm and point resolution = 0.17 nm) and a ***JEOL JEM 2100F, FEG*** (Cs = 0.5 mm, Cc = 1.1 mm and point resolution = 0.19 nm), both with CCD camera (Stockholm University, Arrhenius Laboratory).
- Energy filtered transmission electron microscopy (EFTEM) with a ***JEOL JEM 3000F*** field emission gun TEM (Oxford University, Department of Materials), with a post-column Gatan GIF 2000 imaging spectrometer with CCD camera and ultrahigh-resolution configuration (Cs = 0.60 mm and point resolution = 0.17 nm).

3. Results and discussion

The XRD patterns of the consolidated materials (HC1–HC4) in the 2Θ range 30–65° are shown in Fig. 1, where the peaks for the ceramic and binder phases are depicted. The lattice parameter, a, of the TiC_xN_y ceramic phase (*fcc*-cubic symmetry *Fm*-3*m* space group) was calculated from the whole set of peaks of the XRD diagram (30–130° 2Θ) by using the Fullprof computer program.[14] Assuming that the solid solution was stoichiometric ($x + y = 1$), the corresponding stoichiometry, i.e., the x and y values, was calculated by the Vegard's law obtained from the following JCPDS data files: TiN (38-1420), $TiC_{0.3}N_{0.7}$ (42-1488), $TiC_{0.7}N_{0.3}$ (42-1489), and TiC (32-1383). The obtained data and the nature of the binder phase observed by XRD are presented in Table 1.

It is interesting to note that elemental Ni and Co (the starting reactants) were not detected by XRD after sintering and that the binder phases identified by XRD were, in fact, Ni–Ti or Co–Ti intermetallics. Therefore, the correct name for our consolidated materials is *ceramic–intermetallic composites* instead of ceramic–metal composites. $NiTi_2$ (cubic system *Fd*-3*m*, $a = 11.2780$ Å) is formed in the HC1 composite (Fig. 1a), Ni_3Ti with a hexagonal symmetry (*P*63/*mmc*; $a = 5.0930$ Å, $c = 8.3200$ Å) in the HC3 composite (Fig. 1c), and Co_3Ti with a cubic symmetry (*Pm*3*m*; $a = 3.6140$ Å) in the HC4 composite (Fig. 1d). However, in the HC2 composite, the nature of the intermetallic phase is not so clear (Fig. 1b). It seems that Ni_3Ti is formed, but the presence of another phase cannot be excluded (marked with?).

Representative micrographs obtained by SEM and TEM for the HC1 and HC2 composites (HC3 and HC4 are very similar to HC2 in terms of microstructure) are shown in Fig. 2. The first two (Fig. 2a and b) correspond to SEM images obtained by secondary electrons (Philips XL-30 microscope). The next four images were obtained by HRSEM with secondary (Fig. 2c and d) and backscattered (Fig. 2e and f) electrons (Hitachi S5200 microscope). Secondary electrons allow us to see the

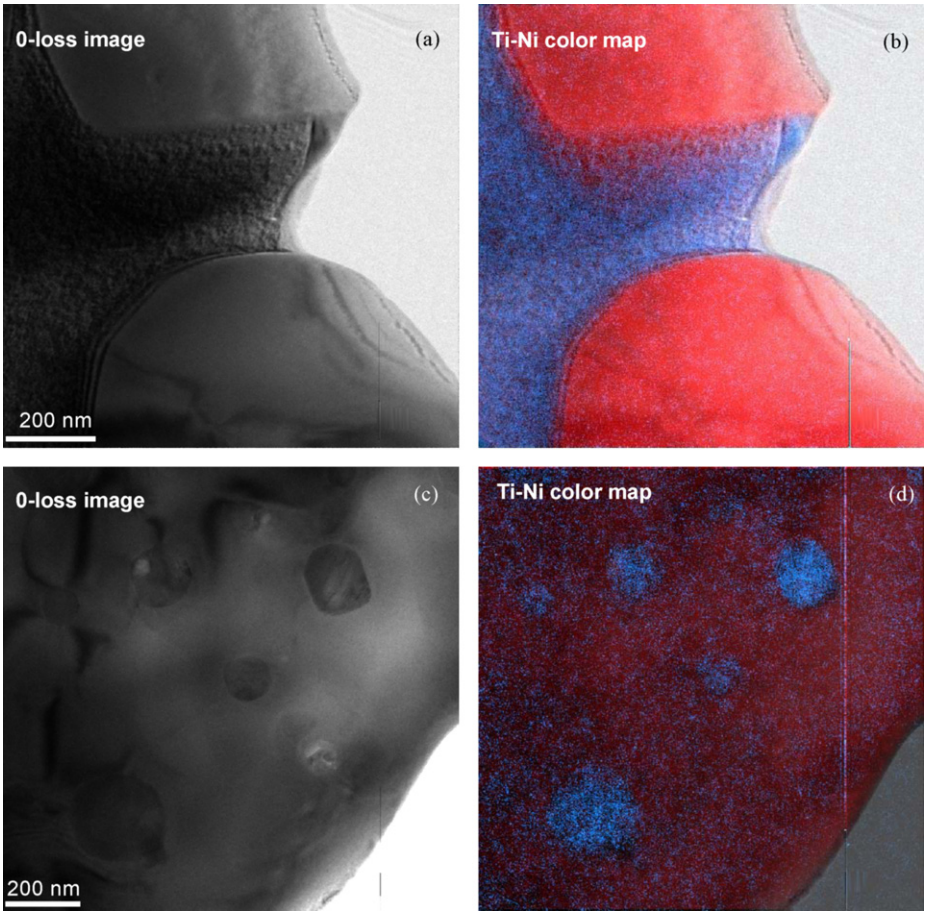

Fig. 3. EFTEM images of two different areas corresponding to HC2 composite. (a and c) 0-loss images and (b and d) Ti–Ni (red–blue) color maps.

morphology, whereas the backscattered electrons clearly show the phase distribution of the two components of the composites due to differences in terms of contrast. Indeed, the ceramic phase has a dark contrast, whereas the intermetallic binder has a lighter one. The last two pictures (Fig. 2g and h) correspond to TEM images (Philips CM200), where the ceramic particles appear with a lighter contrast than the intermetallic binder ones. Note that the contrast in the bright field TEM micrographs is reversed as compared to the scanning electron micrographs. It is worth remarking that in CH1 sample (Fig. 2g) the white background in the micrograph corresponds with holes. It seems to be that during the process of TEM sample preparation (ion milling) the binder phase was removed creating those holes. However, in CH2 sample (Fig. 2h) it is very clear that the darker regions are the binder phase and the grey particles are the ceramic phase.

These micrographs illustrate the composite microstructure consisting of ceramic particles surrounded by the binder phase. The contact between ceramic particles also produces a binder phase at triple point junctions. Two clear differences in terms of size and shape can be seen between HC1 and the other composites. The ceramic particle size is larger in HC1 (5–10 μm), and all the particles are rounded (Fig. 2a, c, e and g). However, in

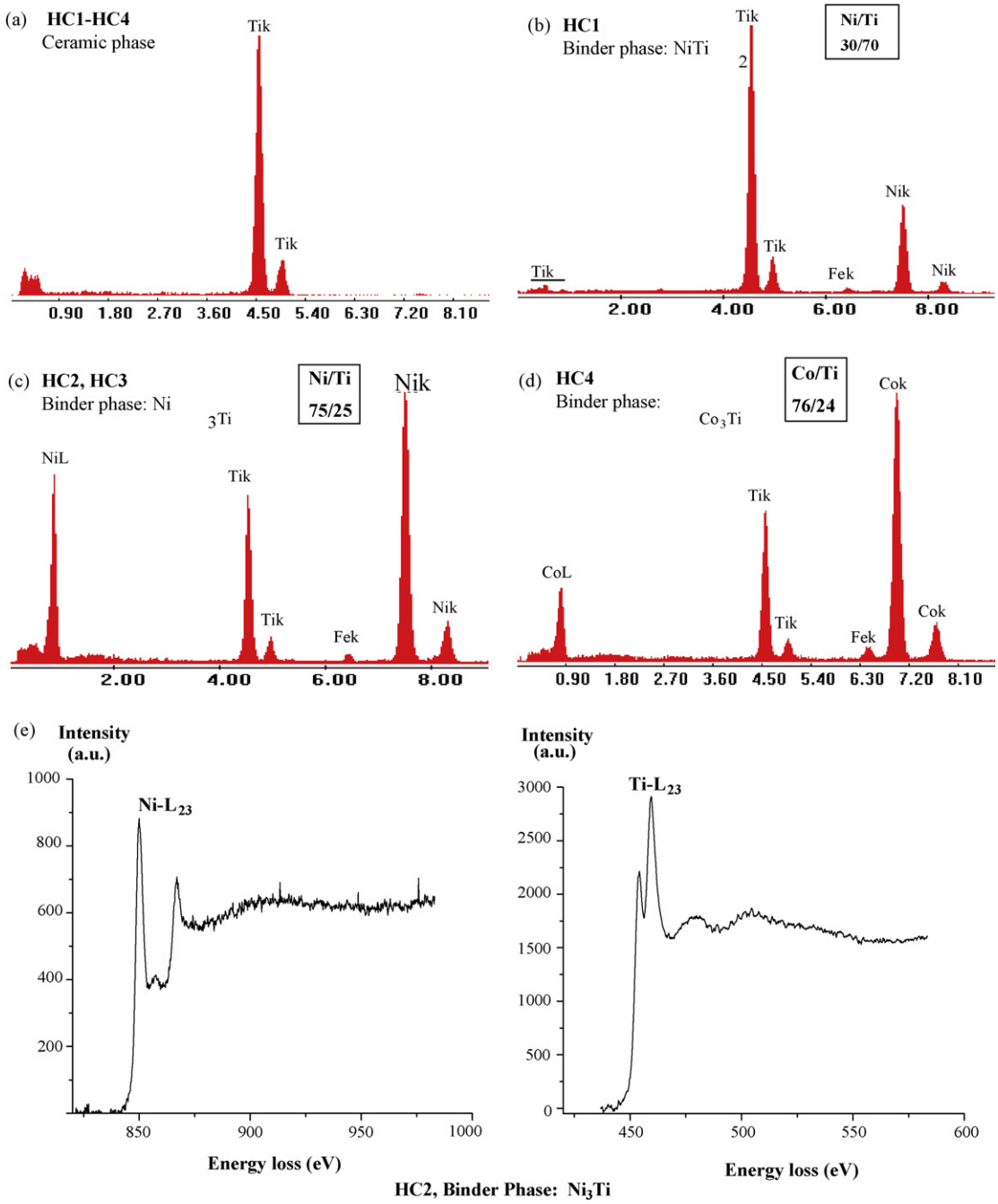

Fig. 4. EDX spectra found for the ceramic (a) and binder phases (b–d) in the four composites. (e) EELS spectra (Ni L_{23}-edge and Ti L_{23}-edge) corresponding to the binder phase Ni_3Ti found in the HC2 composite.

the other three composites the ceramic particle size is smaller (1–5 μm); the smallest particles are rounded, while the largest ones are faceted (Fig. 2b, d, f and h). Another clear difference is the fact that only the HC2–HC4 composites present small inclusions within large ceramic particles (Fig. 2b, f and h). The contrast of these inclusions (with a light contrast in SEM and dark contrast in TEM images) suggests that such particles can either be metallic or intermetallic. However, it was not possible to confirm the composition by EDX analysis (in SEM or TEM) due to their small size (10–20 nm), smaller than the electron beam size. This feature can be explained by the fact that the larger particles have grown from the smaller ones by a coalescence process leaving small inclusions of binder inside the ceramic grains. The differences in microstructure could be due to the chemical composition of the ceramic phase that is richer in nitrogen for HC1 ($TiC_{0.36}N_{0.64}$) than for the other ones (e.g., $TiC_{0.75}N_{0.25}$ for HC2), resulting in a growth characterized by a solution-reprecipitation process instead of coalescence.

The morphology and composition of the composites were also confirmed by EFTEM, and the results corresponding to the HC2 composite are depicted in Fig. 3 (JEOL JEM 3000F FEG microscope). It is easy to visualize how the Ti (red color) and Ni (blue color) were distributed through the material in two different areas. The 0-loss images (Fig. 3a and c) and the Ti–Ni (red–blue) color maps (Fig. 3b and d) for both areas are shown. The first color map (Fig. 3b) shows that the binder phase was distributed between the ceramic grains, embedding them. This result is in agreement with the SEM and TEM analyses. The other color map (Fig. 3d) shows the existence of small particles embedded in the ceramic phase and provides slightly more information than the SEM and TEM micrographs. Indeed, the composition map confirms that the small particles are formed by the binder phase.

EDX analysis by SEM and TEM was performed to confirm the composition of the ceramic particles and the intermetallic binder areas. Representative spectra for all composites obtained by TEM (Philips CM200 microscope) are given in Fig. 4. In the ceramic phase, only Ti was detected (Fig. 4a; it was not possible to analyze C and N with the available equipment), and Ti–Ni or Ti–Co, were observed in the binder areas (Fig. 4b–d). The presence of Fe in the EDX spectra can be explained by the fact that the MSR synthesis was carried out with tempered steel milling bowls and balls.

The composition of the binder, as determined by standardless EDX analysis and presented in each spectrum (Fig. 4b–d), is in agreement with the composition of the phases found by XRD analysis. The binder composition was also analyzed by EELS for the HC2 material. The corresponding EELS spectra belonging to the Ni_3Ti binder phase are presented in Fig. 4e, showing the Ti and Ni L_{23}-edges with a ratio of Ni/Ti of 3/1.

The different intermetallic phases were also identified by ED analysis (TEM Philips CM200 microscope). $NiTi_2$ (cubic

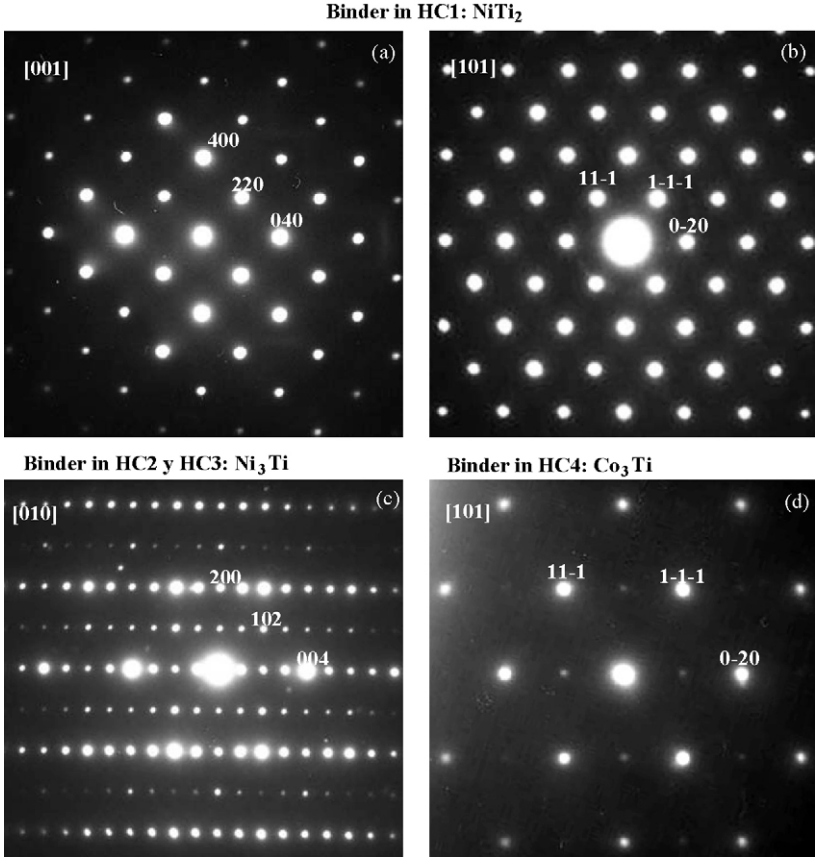

Fig. 5. ED patterns along the (a) [0 0 1] and (b) [1 0 1] corresponding to $NiTi_2$ in the HC1 composite. (c) ED pattern along the [0 1 0] corresponding to Ni_3Ti in HC2 and HC3 composites. (d) ED pattern along the [1 0 1] corresponding to Co_3Ti in HC4 composite.

structure and *Fd*3*m* space group) was observed in the HC1 composite, and the zone axes along [0 0 1] and [1 0 1] are presented in Fig. 5a and b. Ni_3Ti (hexagonal structure and *P*63/*mmc* space group) was found in the HC2 and HC3 composites. The ED pattern along [0 1 0] can be seen in Fig. 5c. Co_3Ti (cubic structure and *Pm*-3*m* space group) was analyzed by ED in the HC4 composite, and the [1 1 0] zone axis is depicted in Fig. 5d.

Besides the ED patterns matching with Ni_3Ti, other ED patterns that do not correspond to intermetallic compounds reported in the literature were also found in the HC2 composite (Fig. 6). This new Ni–Ti intermetallic phase displayed an EDX spectrum with a Ni/Ti ratio of 2/1 (Fig. 6e). Four ED patterns obtained in different orientations and corresponding to the same binder crystal are presented in Fig. 6a–d. Measurements of the inter-planar spacing and angles between them of the different ED patterns allowed us to elucidate a cubic structure with a large lattice parameter close to 8.7 Å. Taking into account this cubic cell, the zone axes of the ED patterns correspond to [0 0 1], [0 1 1], [1 0 2], and [2 1 1]. ED has shown the presence of a new binder intermetallic phase that may be a meta-stable phase formed in

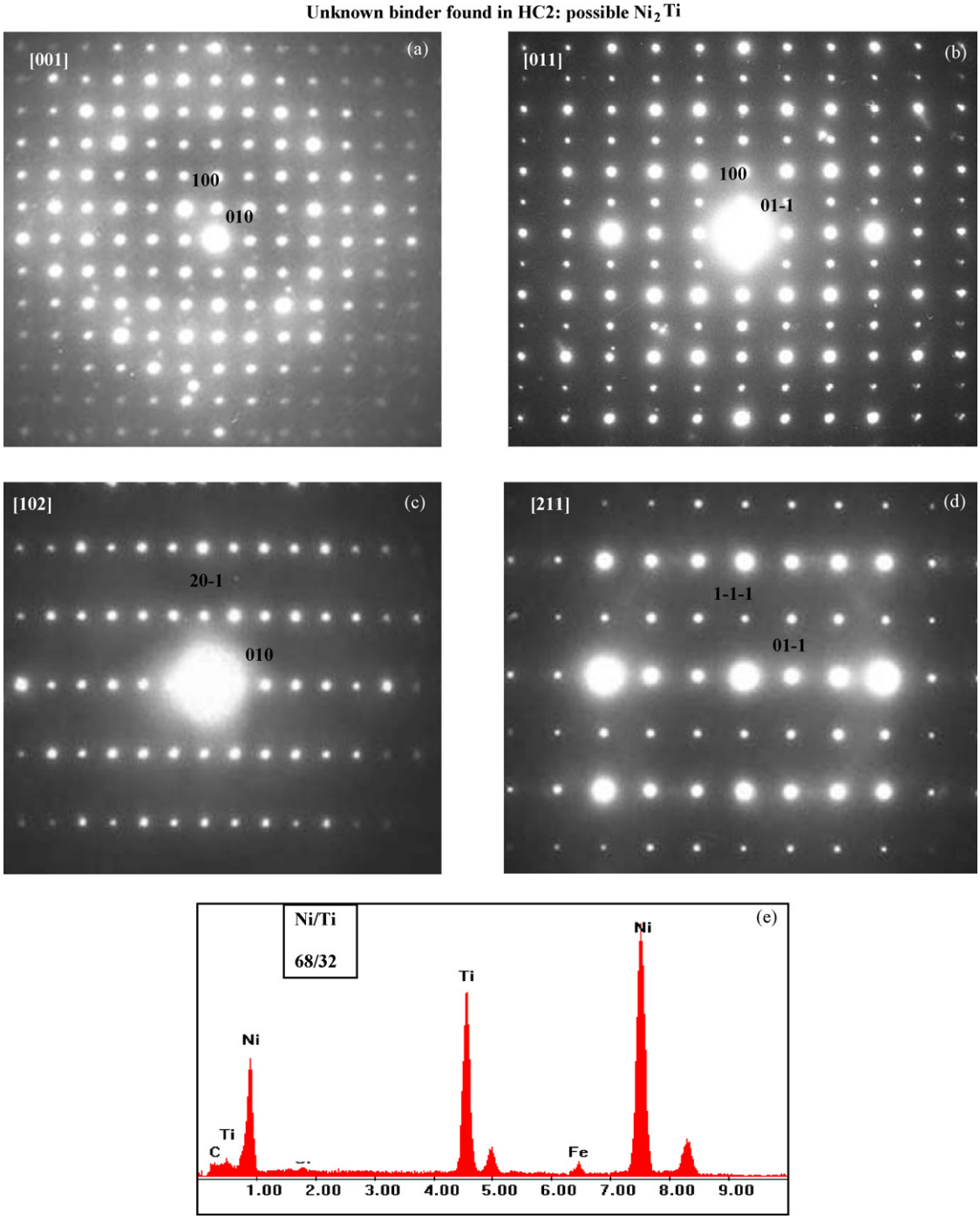

Fig. 6. ED patterns along the (a) [0 0 1], (b) [0 1 −1], (c) [1 0 −2], and (d) [2 −1 1] corresponding to a new Ti–Ni intermetallic phase found in the HC2 composite. (f) EDX spectra corresponding to this compound.

the consolidation process. This new phase was not detected by X-ray diffraction analysis, probably due to the small volume. However, this phase was found several times in the HC2 composite by TEM, allowing the determination of the cell parameters. It was not possible to determine the structure (Ti and Ni atom positions) because the crystals were not thin enough to obtain HRTEM images of good quality.

Microanalysis measurements performed in cermets always detect some amount of titanium in solution with the metal binder.[15] However, only a few papers have reported the presence

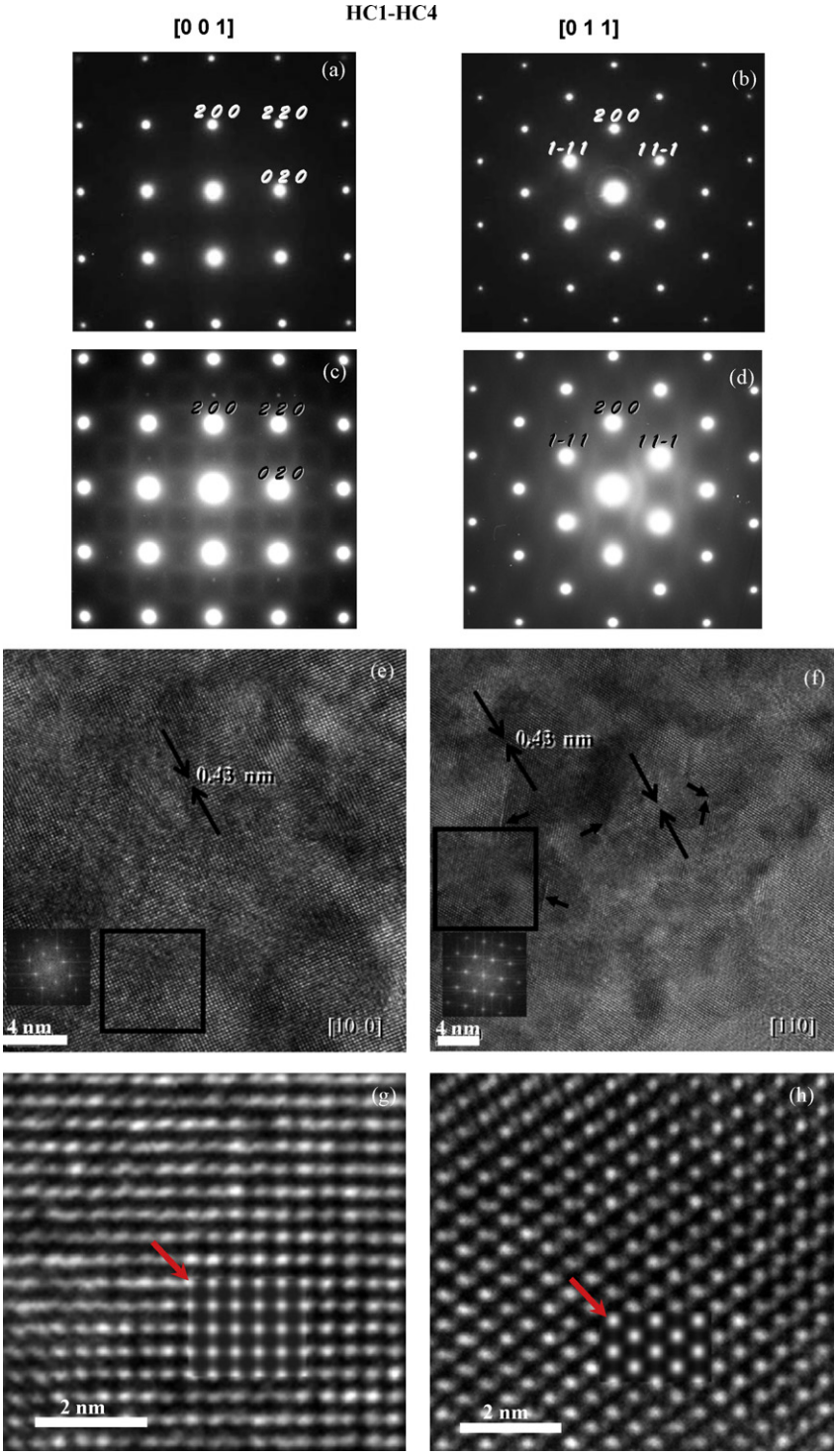

Fig. 7. ED and HRTEM representative results for the ceramic phase in all cermets. ED patterns along the (a) [0 0 1] and (b) [0 1 1] zone axes, (c) and (d) the same axes showing diffuse scattering. (e) and (f) HRTEM images along both axes, d_{100} spacing is marked in both images; in (f) image some defects are arrowed. Insets correspond to the FFT (using Digital Micrograph program) of the square areas. (g) and (h) Enlargements of the above images, the insets marked with arrows show the simulated images along both [0 0 1] and [0 1 1] directions.

of intermetallic phases in Ti-based cermets.[16,17] In these cases, the intermetallic phase was identified as small precipitates embedded in the metal binder. The particles were formed as a consequence of the dissolution of Ti from the ceramic phase into the metal binder during the liquid phase sintering and the subsequent precipitation during the cooling step. However, in our case, the entire binder in the different composites has an intermetallic structure. Taking into account the solubility of TiC_xN_y in liquid binder metals at 1400 °C,[2] it is not realistic to assume that, during the liquid phase sintering, the amount of Ti in the binder is sufficient to induce crystallization from an intermetallic phase melt. Thus, a different explanation is necessary to clarify our results.

Some authors have shown that it is possible to form intermetallic-ceramic composites by SHS reactions from mixtures of Ni, Ti, and C, providing an excess of Ti in the reactant mixture.[18,19] When the combustion process to obtain TiC_x takes place, the Ti surplus forms intermetallic phases with the metallic Ni. In our case, the reactant mixtures present a Ti/C atomic ratio higher than 1, and, as the MSR method is a combustion reaction, the formation of intermetallic phases during the synthesis process is possible. This could be observed for the HC1 powdered composite with a high Ti content in the starting mixture (Ti/C atomic ratio of 1:0.25), where Ti from the incomplete combustion and Ti_2Ni were detected by XRD.[10] The presence of intermetallic phases in the different composites also explains why the TiC_xN_y ceramic phase has a chemical composition richer in C than would be expected from the starting Ti/C atomic ratio.

ED and HRTEM representative results found for the ceramic phase in the four composites are given in Fig. 7 (JEOL JEM 3010 and 2100F FEG). The ED study of the ceramic particles in the HC1–HC4 composites shows that not all the crystals are exactly the same in terms of structure, as can be seen along the [1 0 0] and [1 1 0] zone axes (Fig. 7a–d). Some of the ED patterns (Fig. 7a and b) can be perfectly assigned to the cubic system *Fm*-3*m* space group, whereas other ED patterns (Fig. 7c and d) present additional periodic diffuse intensity distribution (found for all four composites). The diffuse scattering in the ED patterns is produced by short-range order (SRO) and it is possible to detect because each individual crystallite was analysed. The X-ray diffraction technique gives information of the average structure; therefore it is not possible to detect SRO information.

This feature is known for TiC and TiN compounds and is caused by the ordering of vacancies in the C and N cubic sublattices, respectively.[20–22] However, in our case, it is a little more complicated because the anionic sublattice is formed by a mixture of C and N (the ceramic phase is a solid solution of TiC and TiN). Therefore, the short-range order can be caused by a sequence of C and N atom positions or by a sequence of vacancies and C and N atom positions. Thus, they can all form certain order domains and lead to places of diffuse intensity and superstructures spots in the ED patterns.

HRTEM images along the above zone axes (Fig. 7e and f) in regions where the ED patterns display additional periodic diffuse intensity distribution do not reveal a short-range order (SRO), even though some areas of the images show different contrast. This is probably due to a lack of order and some other defects

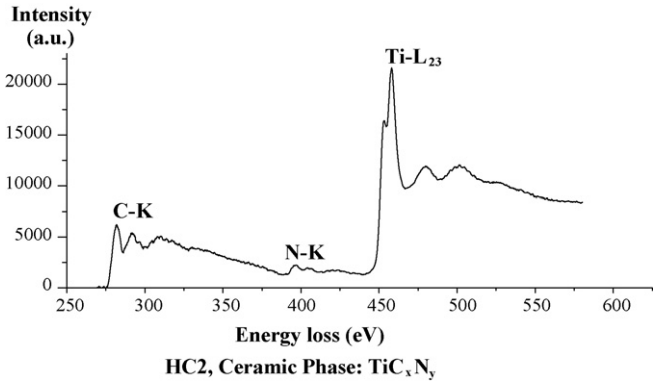

Fig. 8. EELS spectra corresponding to the ceramic phase of the HC2 composite showing the C K-edge, N K-edge, and Ti L_{23}-edge. The background was only removed from the carbon edge.

(arrowed in Fig. 6f). $d_{1\,0\,0}$ spacing is indicated in both images. In order to find the SRO in the areas with different contrast, a Fast Fourier Transform (using the Digital Micrograph program) was applied to the black square marked areas in Fig. 7e and f, to get the calculated diffractograms. The results are depicted on the insets (Fig. 6e and f left-down), but only the *fcc*-cubic spots are shown. Fig. 7g and h, correspond to enlargements of Fig. 7e and f, respectively. Both figures are matched with simulated images (insets marked with arrows) along the two projections ([1 0 0] and [1 1 0]) by the JEMS program using atomic positions and parameters of the *fcc*-cubic structure. The contrast of the experimental and simulated images for both structure orientations are in good agreement.

In order to clarify the C/N composition in the ceramic phase of these composites, electron energy-loss spectroscopy (EELS) was applied to the crystals where diffuse scattering was found. A representative spectrum of the HC2 composite is presented in Fig. 8, showing the C K-edge, N K-edge, and Ti L_{23}-edge. It is worth mentioning that the Ti L_{23}-edge displays a different shape in the ceramic (Fig. 8) and binder (Fig. 4e) phases. This is due to the structure and the Ti bonds in each case. Semi-quantitative analysis of C and N was carried out, using TiC and TiN as standards. The obtained results seem to indicate that the C:N ratio is extremely near to the stoichiometric one. However, many spectra have to be analyzed to obtain more precise average values. Additionally, a more accurate EELS spectrometer is currently used to obtain new spectra. The obtained results, as well as a diffuse scattering ED analysis will be presented in the future.

4. Conclusions

TiC_xN_y/Ti–Ni and TiC_xN_y/Ti–Co composites (HC1–HC4) have been fully microcharacterized using microscopic techniques. SEM and TEM micrographs have shown the differences in morphology and size of the ceramic grain and the binder intermetallic distribution between HC1 and other composites. The binder was formed by an intermetallic compound, joining the ceramic grains of 5–10 μm in size in HC1 and 1–5 μm in size in HC2–HC4. Small particles of binder embedded in ceramic

grains, as revealed by EFTEM images, were only found in the HC2–HC4 composites. Two results could only be obtained by microscopic techniques and not by XRD analysis. The first one was related to a new intermetallic compound with a composition close to Ni_2Ti and a cubic structure ($a = 8.7$ Å). This compound was only found in the HC2 composite by ED and EDS analyses. The second result was that, in all the composites, diffuse scattering from possible atomic or vacancy short-range order in the anionic sublattice (C and N) was observed. Finally, we would like to emphasize the importance of using microscopic techniques to fully characterize composite materials in order to understand their properties and future applications.

Acknowledgements

Supported by the Spanish Government MAT2006-04911, PIE 2007601026 and by the European Union under the Framework 6 program under the ESTEEM contract 026019 (Oxford University). We thanks Prof. G. Svensson for inviting M.J. Sayagués to his department (Structural Chemistry at Stockholm University) and allow the use of HRTEM facilities.

References

1. Pastor H. Titanium carbonitride-based alloy for cutting tools. *Mater Sci Eng A* 1988;**105–106**:401–9.
2. Ettmayer P, Kolaska H, Lengauer W, Dreyer K. Ti(C, N) cermets-metallurgy and properties. *Int J Refract Met Hard Mater* 1995;**13**:343–51.
3. Zhang S. Material development of titanium carbonitride-based cermets for machining application. *Key Eng Mater* 1998;**13**:521–43.
4. Lenguaguer W, Winder S, Aigner K, Ettmayer P, Gullou A, Debuigne J, Groboth G. Solid state properties of group IVb carbonitrides. *J Alloys Compd* 1995;**217**:137–47.
5. Yan Q, Lenguaguer W, Koch T, Scheerer M, Smid I. Hardness and elastic properties of $Ti(C_xN_{1-x})$, $Zr(C_xN_{1-x})$ and $Hf(C_xN_{1-x})$. *J Alloys Compd* 2000;**309**:L5–9.
6. Fukuara M, Mitami H. Mechanism of grain growth in Ti(C, N)-Ni sintered alloys. *Powder Metall* 1982;**25**:62.
7. Qi F, Kang S. A study on microstructural changes in Ti(C, N)-NbC-Ni cermets. *Mater Sci Eng A* 1998;**251**:276–85.
8. Jeon ET, Joardar J, Kang S. Microstructure and tribo-mechanical properties of ultrafine Ti(CN) cermets. *Int J Refract Met Hard Mater* 2002;**20**: 207–11.
9. Zheng Y, Xiong WH, Liu WJ, Lei W, Yuan QA. Effect of nano addition on the microstructures and mechanical properties of Ti(C, N)-based cermets. *Ceram Int* 2005;**31**:165–70.
10. Córdoba JM, Alcalá MD, Avilés MA, Sayagués MJ, Gotor FJ. New production of TiC_xN_{1-x}-based cermets by one step mechanically induced self-sustaining reaction: powder synthesis and pressureless sintering. *J Eur Ceram Soc* 2008;**28**:2085–98.
11. Córdoba JM, Sayagués MJ, Alcalá MD, Gotor FJ. Synthesis of titanium carbonitride phases by reactive milling of the elemental mixed powders. *J Am Ceram Soc* 2005;**88**:1760–4.
12. Córdoba JM, Sayagués MJ, Alcalá MD, Gotor FJ. Monophasic nanostructured powders of Nb, Ta and Hf carbonitride phases synthesized by mechanically induced self-propagating reaction. *J Am Ceram Soc* 2007;**92**:1760–4.
13. Córdoba JM, Sánchez-López JC, Avilés MA, Alcalá MD, Gotor FJ. Properties of Ti(C, N) cermets synthesized by mechanically induced self-sustaining reaction. *J Eur Ceram Soc* 2009;**29**:1173–82.
14. Rodríguez-Carvaja, J., FULLPROF *program*. February 2006 version, ILL.
15. Heiligers C, Neethlin JH. Crystal structure of the binder phase in a model HfC-TiC-Ni material. *J Alloys Compd* 2008;**453**:222–8.
16. Lindah P, Rolander U, Andrén HO. Atom-probe analysis of the binder phase in TiC-TiN-Mo_2C-(Ni,Co) cermets. *Int J Refract Met Hard Mater* 1993–1994;**12**:115–9.
17. Zackrisson J, Larsson A, Andrén HO. Microstructure of the Ni binder phase in a TiC-Mo_2C-Ni cermet. *Micron* 2001;**32**:707–12.
18. Zaripov NG, Kabirov RR, Bloshenko VN. Structural peculiarities of cermets design based on titanium carbide. Part II. The increase of properties of high-temperature TiC-based cermets by intermetallic strengthening. *J Mater Sci* 1996;**31**:5743–7.
19. Burkes DE, Gottoli G, Moore JJ, Yi HC. Production of Ni_3Ti-TiC_x intermetallic-ceramic composites employing combustion synthesis reactions. *Metall Mater Trans A* 2006;**37**:1045–53.
20. Billingham J, Bell PS, Lewis MH. Vacancy short-range order in substoichiometric transition metal carbides and nitrides with the NaCl structure. I. Electron diffraction studies of short-range ordered compounds. *Acta Cryst A* 1972;**28**:602–6.
21. Savage M, Parth E. Vacancy short-range order in substoichiometric transition metal carbides and nitrides with the NaCl structure. II. Numerical calculation of vacancy arrangement. *Acta Cryst A* 1972;**28**: 607–16.
22. Bursick J, Beatherly GC. Ordering of substoichiometric δ-TiC_x phase in Ti-V-C. *Alloys Phys Stat Sol* 1999;**174**:327–35.